ENERGY TRANSPORT IN 1-D HAMILTONIAN LATTICES: FROM PHYSICS TO ENGINEERING (Non-Analytic Potentials)

Anastasios (Tassos) Bountis
Professor Emeritus, University of Patras, Greece

Lecture at the 30th Summer School on Nonlinear Dynamics and Complexity
Possidi, Chalkidiki, Greece, August 28 - September 8, 2024

Main Collaborators and Contributions

- Dr. Konstantinos Kaloudis, Consiglio Nazionale delle Ricerche, Napoli, Italy
- Prof. Haris Skokos and Dr. Bertin Many Manda, Dept. of Mathematics and Applied Mathematics, University of Cape Town, South Africa.
  In the publications:
- A. Bountis, K. Kaloudis, Th. Oikonomou, B. Many Manda, Ch. Skokos, "Stability Properties of 1-D Hamiltonian Lattices with Non-Analytic Potential", IJBC Volume No. 30, Issue No. 15, Article No. 2030047 (2020).
- Bountis T., Kaloudis K., Shena J., Skokos Ch., and Spitas Ch., "Energy Transport in 1-Dimensional Oscillator Arrays with Hysteretic Damping", Eur. Phys. J. Spec. Top. 231: 225-236 (2022).

Introduction and Motivation

We wish to study mechanical engineering models with non-analytic potentials:

1. 1–D lattices with graphene type interactions.
2. 1–D lattices whose interactions obey Hollomon's law of "work hardening".
3. Periodically forced 1–D lattices with hysteretic damping.

We aim to understand:

- First destabilization of simple periodic orbits (SPOs): Local and global chaos
- Supratransmission and wave packet spreading in nonlinear arrays with hysteretic damping
- Breathers and Breather "arrest" in nonlinear arrays with hysteretic damping

The graphene model

A single graphene oscillator is often described in the literature as a 1–DOF mass-spring system:

$$m\ddot{x} = -Kx + Dx|x|, \quad K > 0, \quad D > 0$$

In the $N-$ particle case, with nearest- neighbor interactions:

Graphene Hamiltonian:

$$\mathcal{H} = \sum_{j=1}^{n} \frac{m_j}{2} \dot{x_j}^2 + \sum_{j=0}^{n} \frac{K}{2} \left(x_{j+1} - x_j\right)^2 - \frac{D}{3}|x_{j+1} - x_j|^3, \tag{1}$$

- K : elastic constant, D : material stiffness, x_j : displacement of the $j-$th particle from its equilibrium position.

and impose fixed boundary conditions: $x_0(t) = x_{n+1}(t) = 0, \forall t.$

Potential energy for the N=2 oscillator system

$$V(\mathbf{x}) = \sum_{i=0}^{N} \frac{K}{2}(x_{i+1} - x_i)^2 - \frac{D}{3}|x_{i+1} - x_i|^3. \tag{2}$$

Clearly, for large displacements, there will be an escape energy, where the lattice is expected to break. Consider, for example, the case $N = 2$:

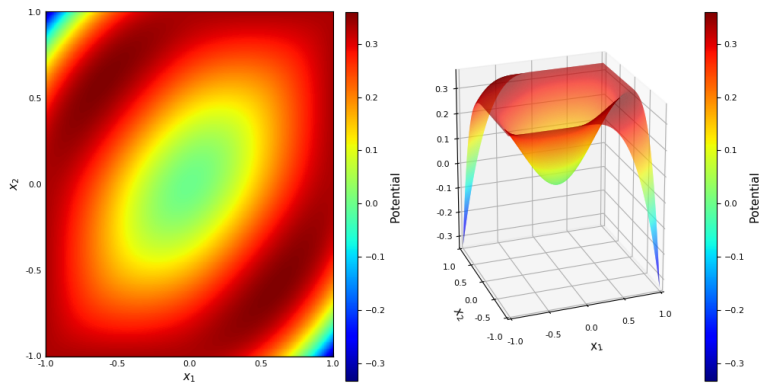

Figure 1: Potential surface of the 2-particle graphene model, with escape energy $E_n^{(c)} = 0.33\ldots$. Left: 2-d cross sections. Right: The 3-d potential surface. The SPOs we will examine later are orbits along symmetry lines

Graphene oscillations are very stable!

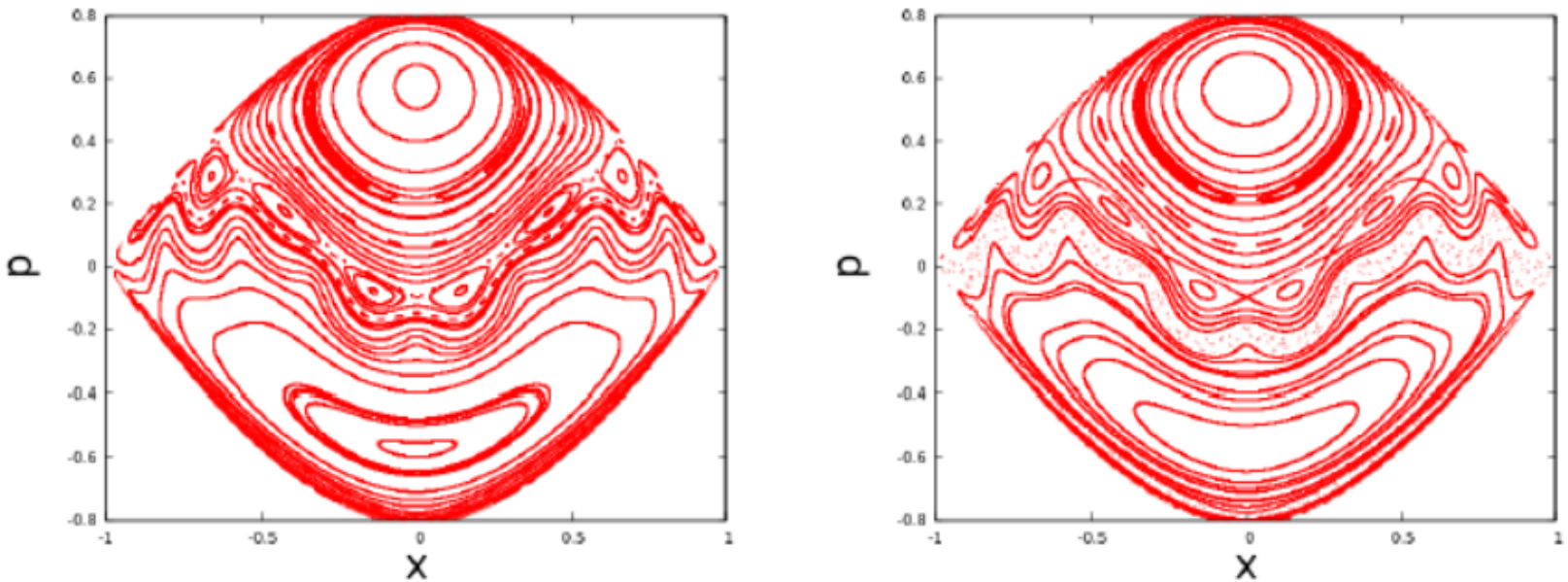

Figure 2: Poincaré Surfaces of Section (PSS) at E=0.3333 and E=0.3334, slightly below and above the escape energy threshold indicate highly stable dynamics! The chaotic regions are very small! The centers of big islands are examples of SPOs.

Examples of Simple Periodic Orbits

FPU N=4 OPM with fixed boundary conditions

FPU N=7 SPO1 with fixed boundary conditions

FPU N=8 SPO2 with fixed boundary conditions

Examples of SPO solutions: The SPO1 is shown in the middle with N=7 oscillators.

Chaos near the middle oscillator of SPO1 $N = 5$

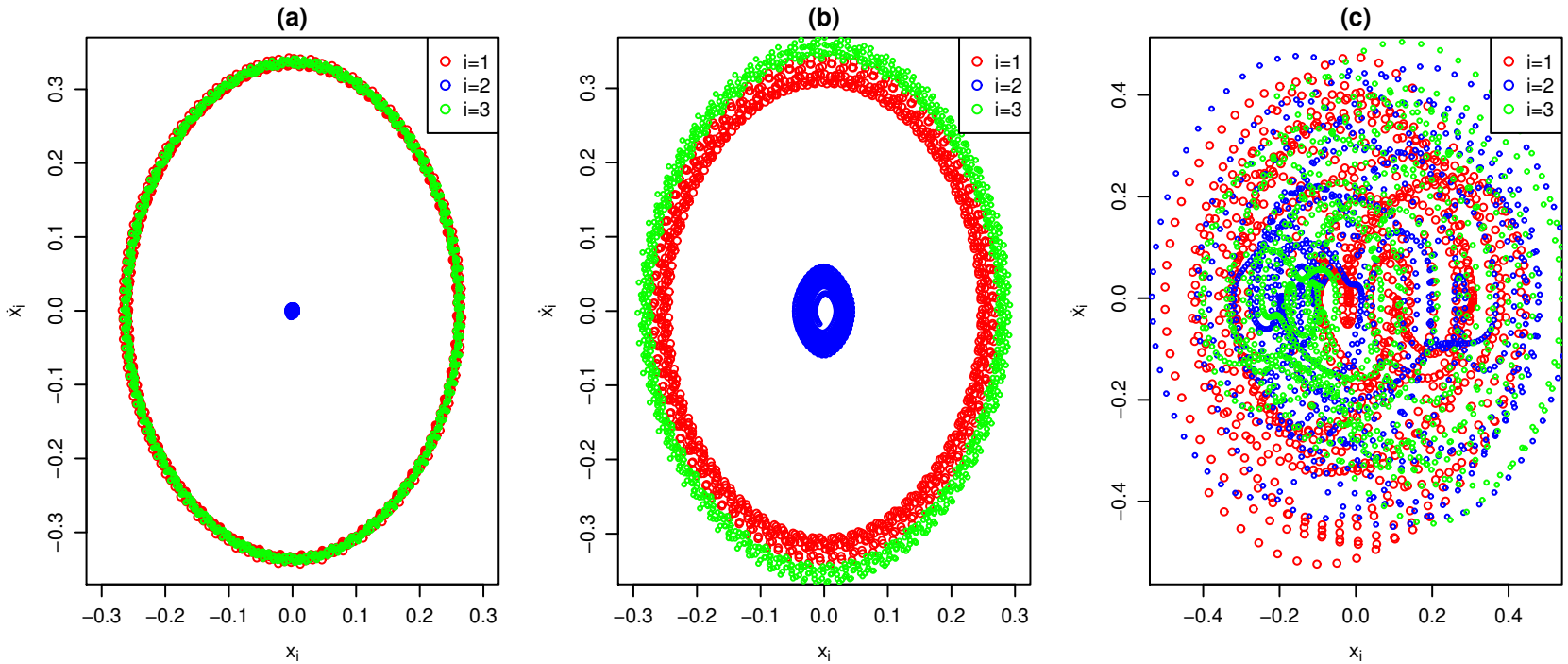

Figure 3: Phase plots $(x_i(t), \dot{x}_i(t))$, for $i \in \{1, 2, 3\}$ at (a) $E = 0.17$ (stability), then right after instability (b) $E = 0.21$ (weak chaos), and (c) $E = 0.22$ (strong chaos), for deviations of the SPO1 mode of the graphene-type Hamiltonian.

Weak and strong chaos near the middle oscillator

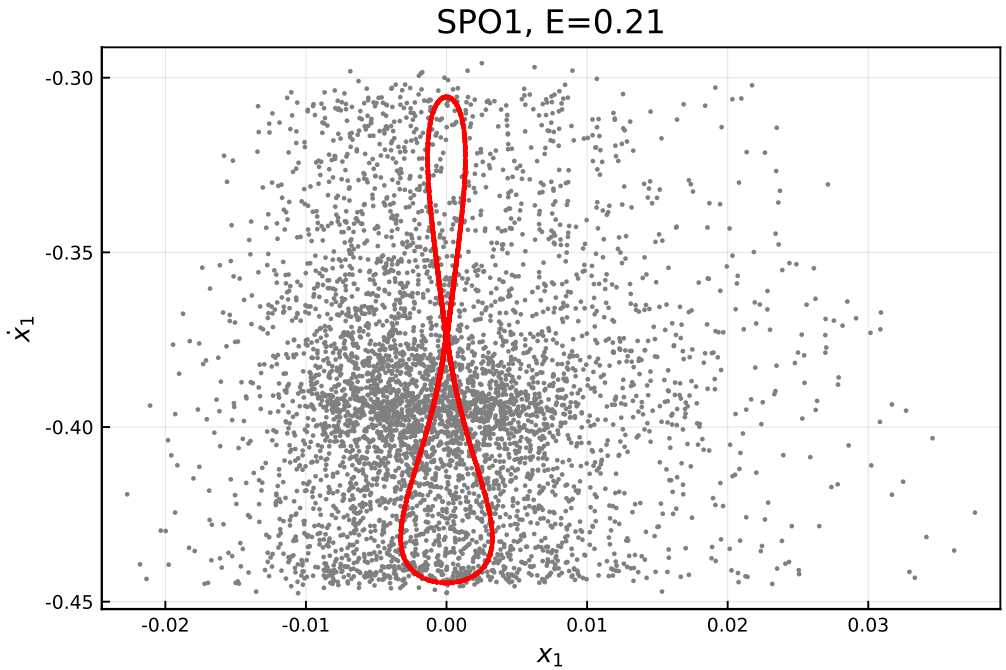

Figure 4: A "figure-8" chaotic orbit near the middle oscillator of an $N = 5$ lattice starting at a distance $|\epsilon| = 10^{-5}$ from the SPO. Note the small - scale ("weak") chaos, while, starting at ($|\epsilon| = 10^{-2}$), the orbits spread over much larger ("strongly") chaotic domains.

Identifying the destabilization of SPO1 for N=5 using the maximal Lyapunov exponent

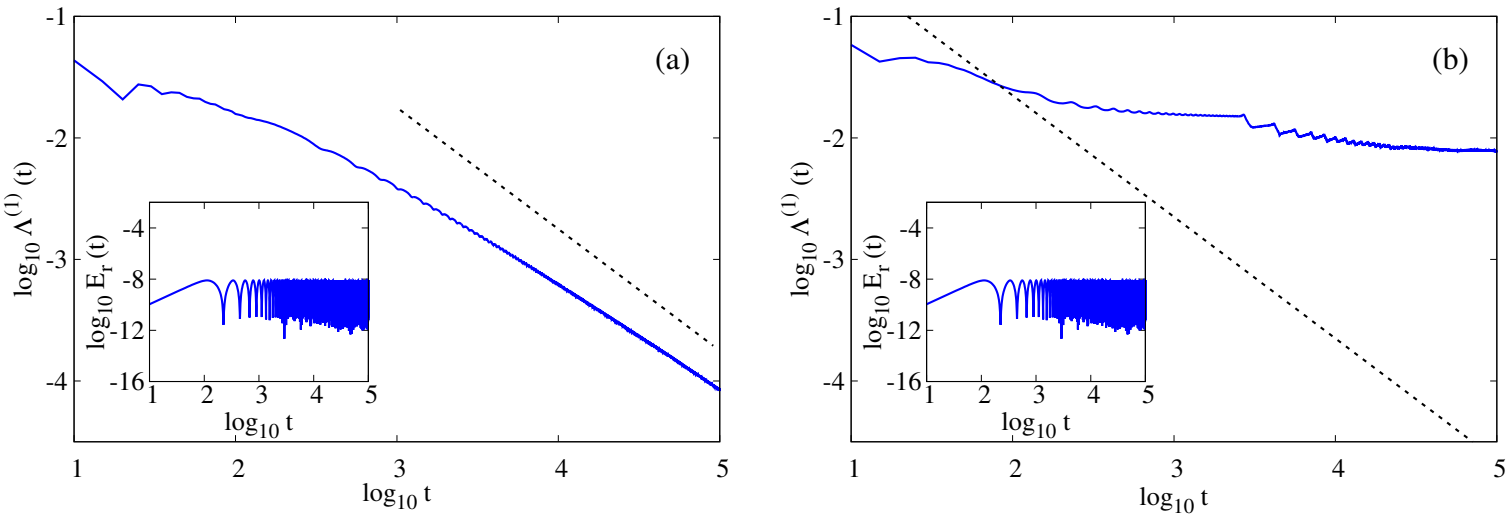

Figure 5: Time evolution (in log-log scale) of the *maximal* Lyapunov exponent for SPO1 at energies (a) $E = 0.1305$, and (b) $E = 0.2130$, below and above of the orbit's first destabilization, for the graphene lattice (1). In both panels the dashed straight line is $\propto t^{-1}$. The inserts show the time evolution of the relative energy error $E_r(t)$.

Distinguishing "weak" from "strong" chaos for N=5 using the spectrum of Lyapunov exponents

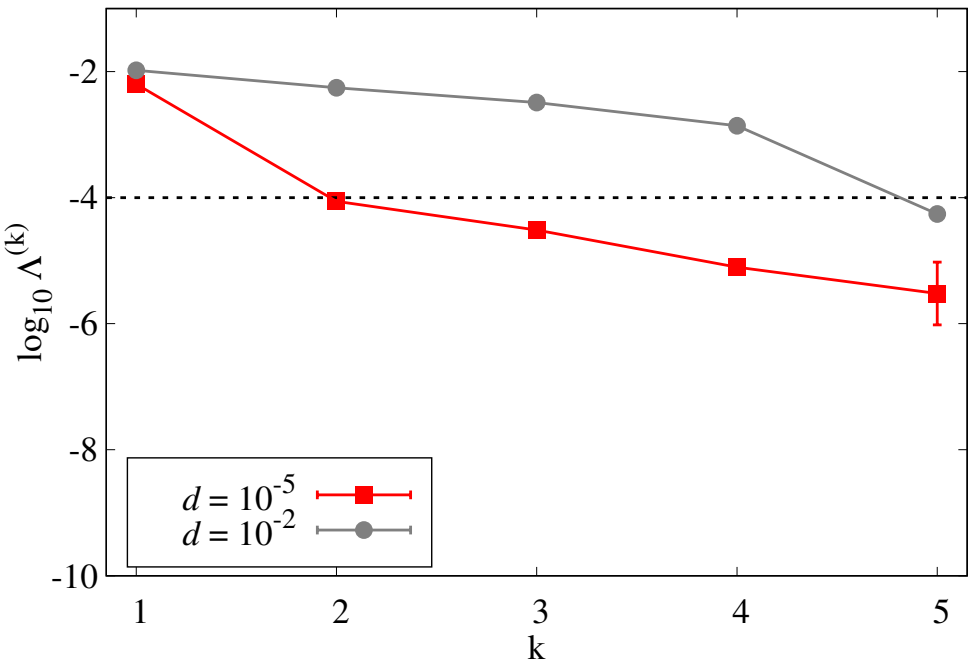

Figure 6: The spectrum of LEs $\Lambda^{(k)}$, $k = 1, 2, 3, 4, 5$, of the "figure-8" (red curve) and the large scale chaos (gray curve) orbits of Fig. 6, at distances $d = 10^{-5}$ and $d = 10^{-2}$ from the SPO1, respectively. The dashed horizontal line represents the level above which we consider a LE to be strongly positive.

Destabilization Energy of SPO1 as N increases

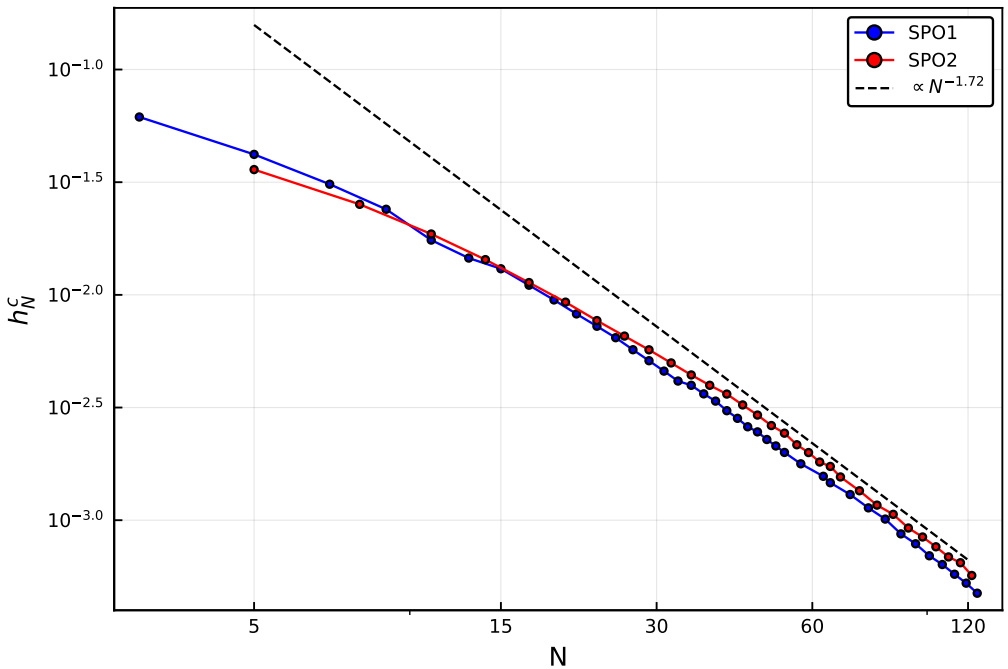

Figure 7: Observe how, as expected, when the number of particles N increases the instability threshold of the SPO1 and SPO2 orbits of the graphene lattice decrease to zero following power laws that tend to coincide.

The surprising Hollomon lattice model!

Hollomon model Hamiltonian:

$$\mathcal{H} = \sum_{j=1}^{n} \frac{m_j}{2} \dot{x}_j^2 + \sum_{j=0}^{n} \frac{K}{2} \left(x_{j+1} - x_j\right)^2 + \frac{\beta}{1+q} |x_{j+1} - x_j|^{1+q}, \qquad (3)$$

- $0 \leq q < 1$ associated with Hollomon's law, will be set to $q = 1/3$.
- $\beta > 0$: no escape, bounded motion.

For small displacements, the Hollomon interactions $\left|x_{j+1} - x_j\right|^{q+1}$, $0 \leq q < 1$, are stronger than the harmonic terms and lead to instability for low energies.
Remarkably, as the energy grows, the harmonic terms become dominant leading to stability of the SPOs!.

SPO1 and SPO2 stabilize at high energy values!

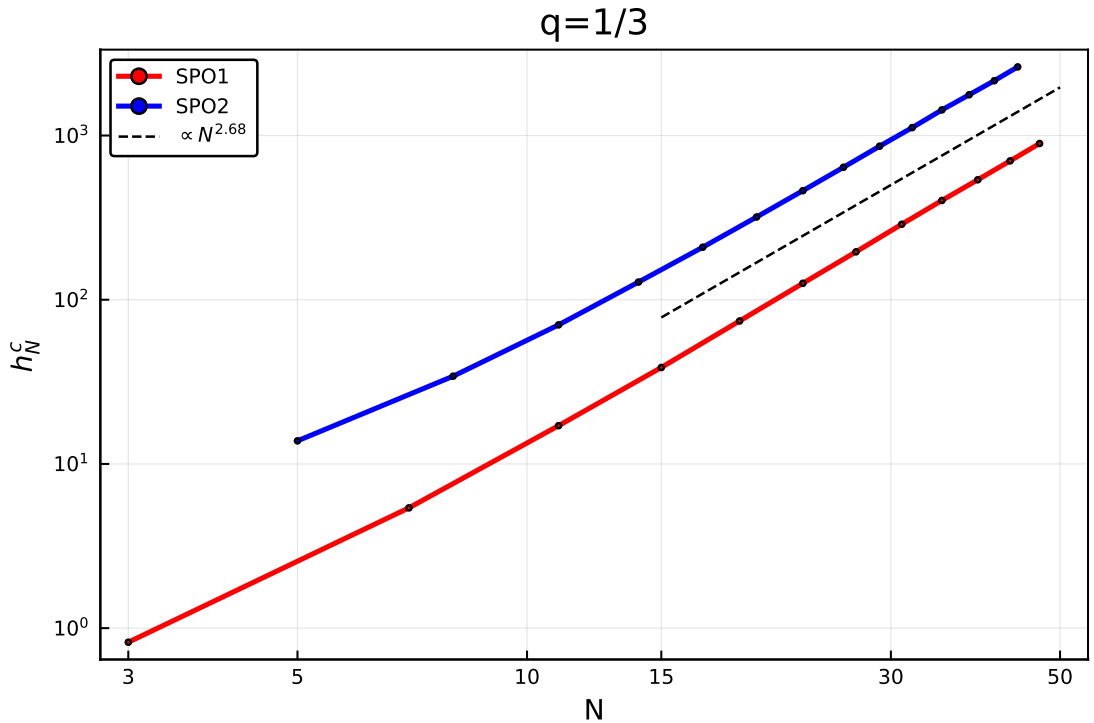

Figure 8: Logarithmic plot of the approximate energies per particle $h_N^c = E_N^c/N$ where the first stabilization of SPO1 and SPO2 occurs, showing a power law behavior of the form $\propto N^\beta$, with $\beta \approx 2.68$ (dashed line).

Model I: Local hysteretic damping with periodic forcing

- Hysteretic damping: Total linear force is not in phase with x(t); energy loss per cycle is independent of the driving frequency of linear oscillations.
- Applications: seismic behavior, composite beam modeling, rotor dynamics and material modeling.

Reid's model (1956)

$$M\ddot{x} + c\left|\frac{x}{\dot{x}}\right|\dot{x} + kx = M\ddot{x} + kx\left(1 + \frac{c}{k}\mathrm{sgn}(x\dot{x})\right) = F\sin\omega t, \qquad (4)$$

where sgn(·) is the sign function, c is the damping coefficient, and k quantifies the (linear) stiffness.

The nonlinear 1 - DOF Reid's model

$$M\ddot{x} + c\left|\frac{x}{\dot{x}}\right|\dot{x} + kx + \epsilon x^3 = f \sin \omega t.$$

- The symmetric cubic nonlinearity allows for no escape of solutions to infinity.
- Relatively high damping → a unique stable periodic solution with period $T^* = 2\pi/\omega$
- Relatively low damping → emergence of stable periodic orbits whose period is a multiple of T^* (forcing period).
- A highly complex basin of attraction emerges.

Basins of attraction

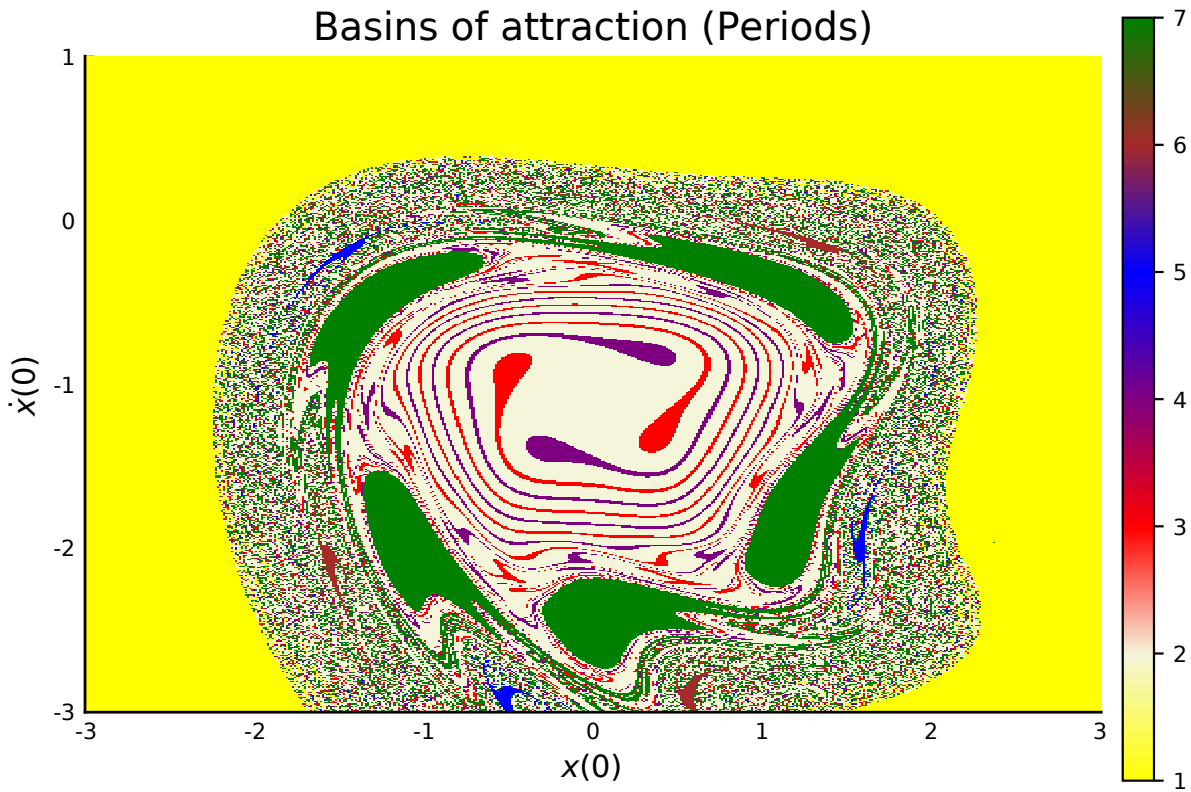

Figure 9: Basins of attraction of the modified Reid's model for parameters $(c, k, f, \omega, \epsilon) = (0.01, 0.3, 1.1, 1.3, 0.1)$. We have used different coloring for orbits with period $T = T^*$ (white), red and purple for $T = 2T^*$, blue for $T = 3T^*$ and green for $T = 5T^*$

Supratransmission in Model I of nonlinear Reid oscillators

Equations of motion for N–DOF system

For $j = 1, \ldots, N$:

$$M\ddot{x}_j = -c\left|x_j\right| \tanh\{\tau \dot{x}_j\} - k\left(-x_{j-1} + 2x_j - x_{j+1}\right) - \epsilon\left(-\left(x_{j+1} - x_j\right)^3 + \left(x_j - x_{j-1}\right)^3\right), \tag{5}$$

subjected to the boundary values at the origin and the end:

$$x_0(t) = f \sin \omega t \quad \text{and } x_{N+1}(t) = 0, \quad t \in \mathcal{T} \subseteq \mathbb{R}+ .$$

Supratransmission of the full Reid's lattice

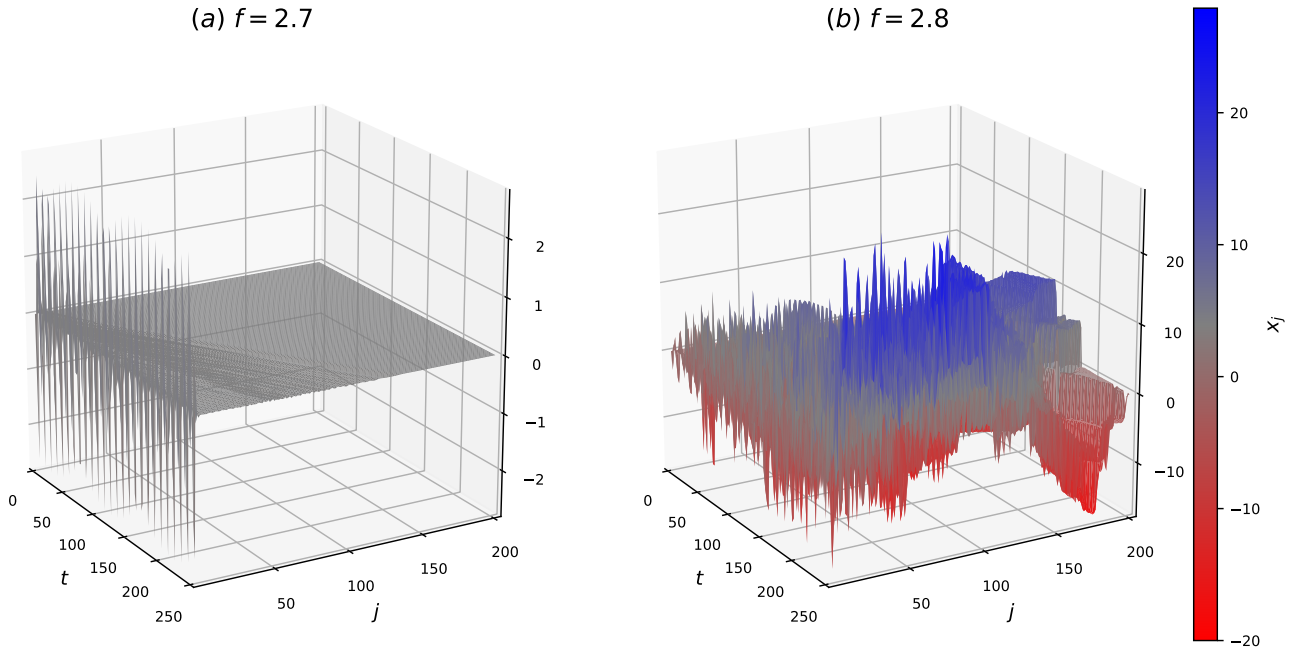

Figure 10: Graphs of the displacement solutions of Eqs. (5) at critical amplitude $2.7 < f < 2.8$, selecting $\omega > 2$ values outside the forbidden band gap, $0 < \omega < 2$.

Damping does not affect Supratransmission!

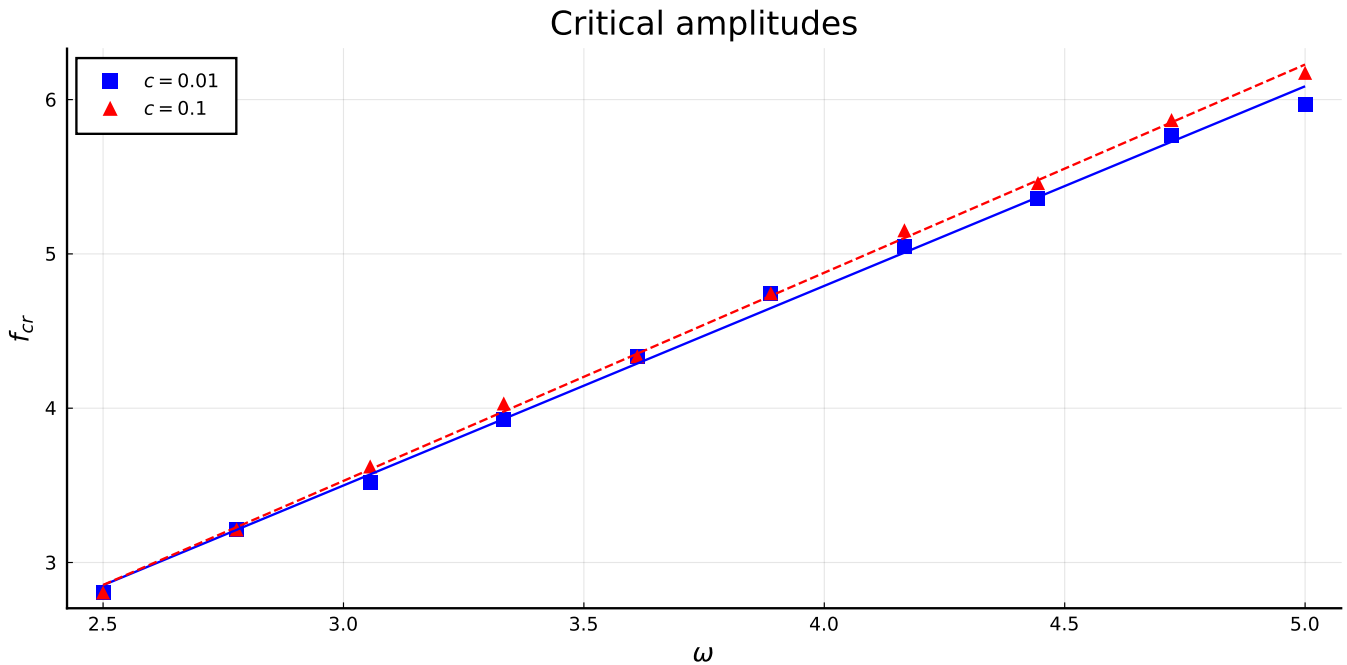

Figure 11: Critical forcing amplitudes f_{cr} of model I as functions of ω, with $(k, \epsilon) = (0.3, 0.1)$. For different damping parameters $c \in \{0.01, 0.1\}$, and $N = 200$ oscillators.

Model II: Non-local hysteretic damping

We now turn to Model II whose hysteretic damping terms are nearest neighbor dependent according to the difference operators $\Delta^- x_j := x_j - x_{j-1}$ and $\Delta^+ x_j := x_j - x_{j+1}$, and similarly, $\Delta^- \dot{x}_j := \dot{x}_j - \dot{x}_{j-1}$ and $\Delta^+ \dot{x}_j := \dot{x}_j - \dot{x}_{j+1}$ for the velocity terms. Thus the equations of motion become

$$\begin{aligned} M\ddot{x}_j + c\left(\Delta^- x_j \operatorname{sgn}(\Delta^- x_j \Delta^- \dot{x}_j) + c\,\Delta^+ x_j \operatorname{sgn}(\Delta^+ x_j \Delta^+ \dot{x}_j)\right) \\ + k\left(\Delta^- x_j + \Delta^+ x_j\right) + \epsilon\left(\left(\Delta^- x_j\right)^3 + \left(\Delta^+ x_j\right)^3\right) = 0 \end{aligned} \tag{6}$$

Model II is subject to the same boundary conditions as model I:

$$x_0(t) = f \sin \omega t \quad \text{and} \quad x_{N+1}(t) = 0, \quad t \in \mathcal{T} \subseteq \mathbb{R}^+ \tag{7}$$

Supratransmission in model II: No difference with model I

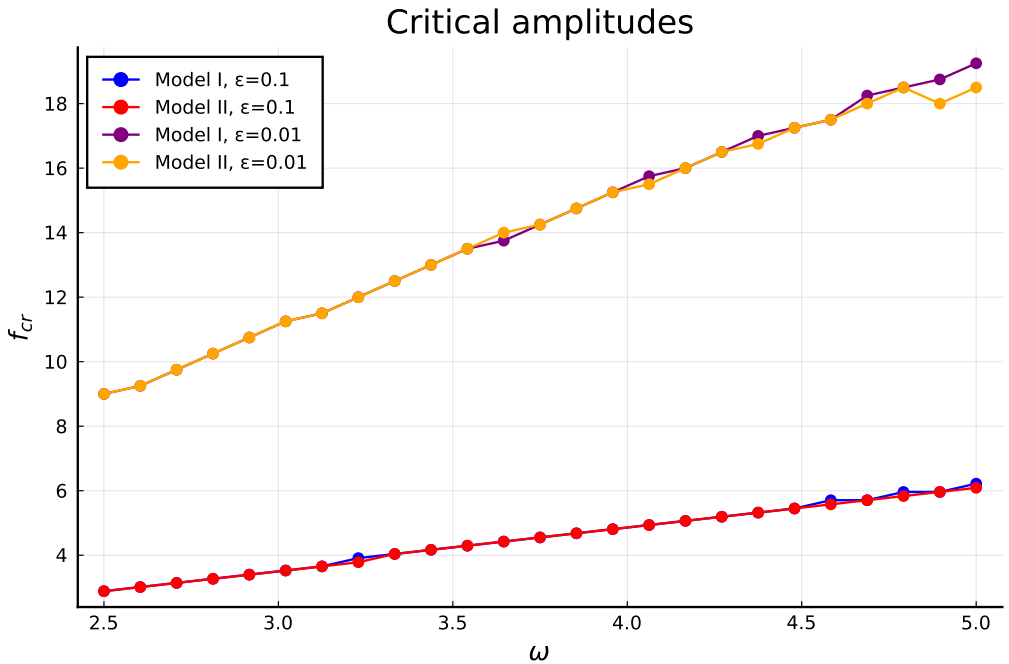

Figure 12: Plots of supratransmission critical amplitudes f_{cr} as functions of the forcing frequency ω for Models I and II, for $\epsilon \in \{0.01, 0.1\}$ and $(k, c) = (0.3, 0.01)$. The curves corresponding to the same ϵ value practically overlap.

New Result: Breather propagation and breather arrest

Recently, we discovered in the mechanical engineering literature (2018 - 2021) several papers discussing the phenomenon of Acoustic Non-reciprocity in mechanical lattices like our own, but with viscous damping.

$\ddot{x}_1 + d\dot{x}_1 + kx_1 + C(x_1 - x_2)^3 = F_0\hat{f}(t)$,

$\ddot{x}_i + d\dot{x}_i + kx_i + C(x_i - x_{i-1})^3 + C(x_i - x_{i+1})^3 = 0$

with initial conditions $x_i(0+) = 0, \dot{x}_i(0+) = 0, i = 1, 2, \ldots, n$ and $\hat{f}(t) = sin(\omega t)$ for $t = [0, \pi/\omega)]$ and zero for $t > \pi/\omega$!

They observed the existence of localized oscillations (breathers), which start from the first few particles and travel down the lattice, for short times and then damp out to zero leading to (breather arrest).

Breathers and breather arrest in our Models I and II

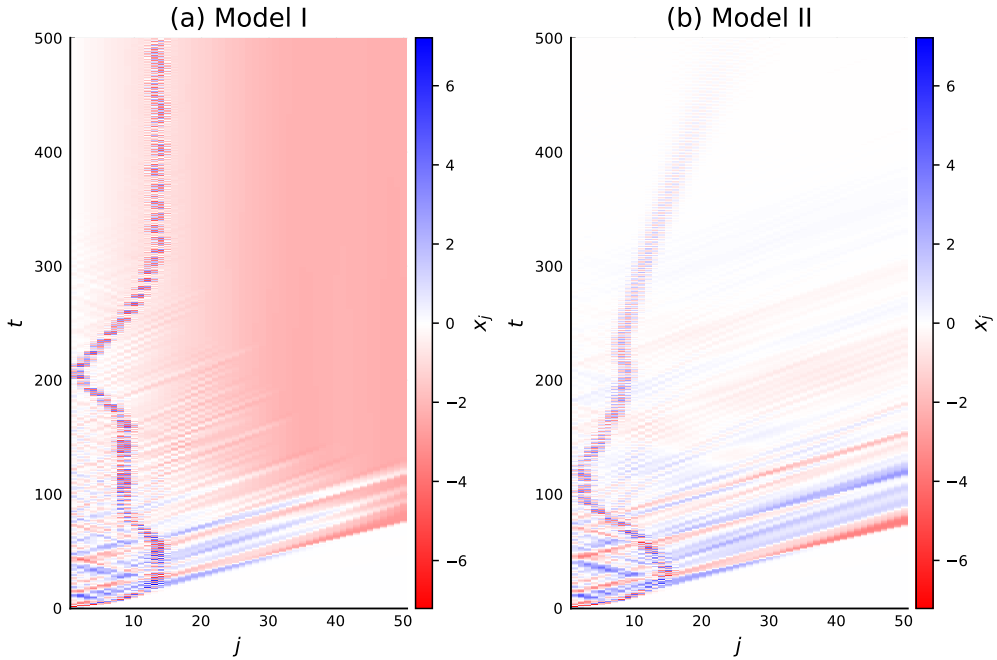

Figure 13: Spatiotemporal evolution of the displacement solutions of the impulsively forced Model I (a) and Model II (b). The parameters are set to $(c, k, f, \omega, \epsilon) = (0.01, 0.3, 3.5, 4, 0.1)$. Only the first 50 of the $N = 200$ particles are depicted.

Breathers and breather arrest in our Models I and II

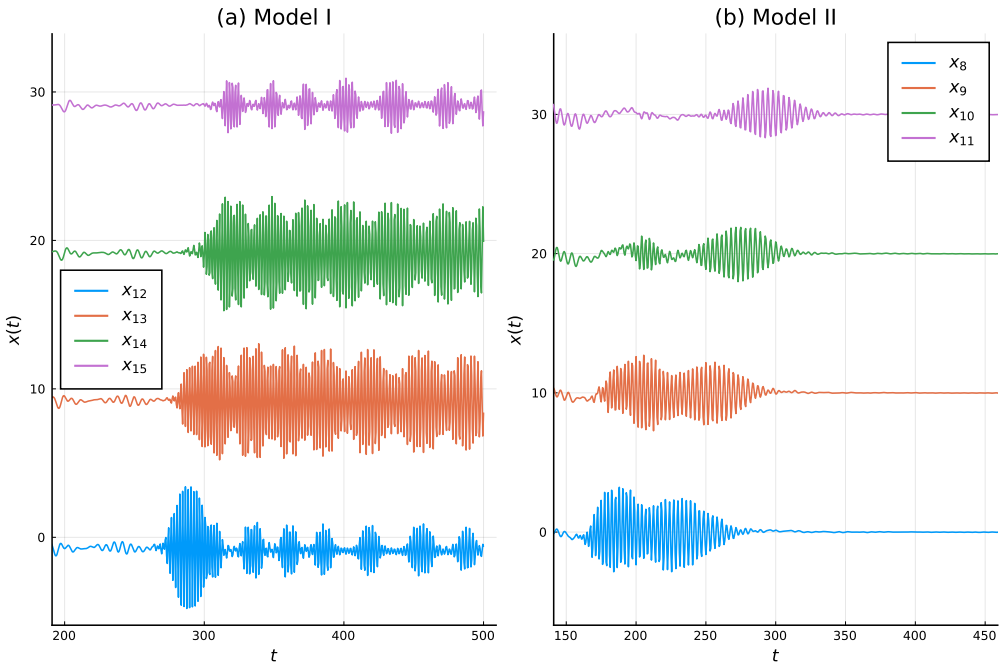

Figure 14: Temporal evolution of the displacement solutions of our impulsively forced Model I (a) and Model II (b) for the same parameters as above. The breather solutions are clearly visible but our results of Model II (non-local hysteretic damping) are closer to the results of models with non-local viscous damping in the literature!

Conclusions of Part I: Analytic potentials

1. In the FPU β– lattice the SPOs we studied are stable at low energies and experience a first destabilization at energies per particle E_N^c/N that decrease, as N increases, by power laws either $\propto N^{-1}$ or $\propto N^{-2}$.
2. In the FPU model chaotic orbits near an SPO that has just destabilized do not immediately spread over large domains in phase space, but remain for long times close to the SPO exhibiting what one might call "weak" chaos
3. In weakly chaotic domains the probability density functions of the orbits follow Tsallis statistics, while in strongly chaotic regimes we observe Boltzmann-Gibbs statistics.
4. In the phenomenon of supratransmission the range of interactions as well as the presence of an on site potential play an important role.

Conclusions of Part II: Non-analytic potentials

1. In the graphene-type lattice the SPOs are stable at low energies and experience a first destabilization at energies per particle E_N^c/N that decrease, as N increases, by power laws with nearly equal exponents, i.e. $\propto N^{-1.72}$.
2. In the graphene model the motion near unstable SPOs does not immediately spread over large domains in phase space, and exhibits what one might call "weak" chaos.
3. The corresponding results for the Hollomon lattice are strikingly different: Both SPO1 and SPO2 are unstable at low energies and first stabilize along curves of the form $E_N^c/N \propto N^{2.68}$, (for an interaction exponent with $q = 1/3$).
4. Reid's lattice of nonlinear oscillators with hysteretic damping exhibits important phenomena like supratransmission and also Breathers and Breather Arrest similar to models with viscous damping.

References


Bountis T., Kaloudis K., Oikonomou T., Manda B.M., Skokos C. (2020)
"Stability properties of 1-Dimensional Hamiltonian lattices with non-analytic potentials", Int. J. Bifurc. Chaos **30**, Issue No. 15, Article No. 2030047 (2020).


Bountis T., Kaloudis K., Spitas C. (2020)
"Periodically forced nonlinear oscillators with hysteretic damping", Journal of Computational Nonlinear Dynamics, **15** (12) 121006 (2020).


Bountis T., Kaloudis K., Shena J., Skokos Ch., and Spitas Ch. (2021)
"Energy transport in one-dimensional oscillator arrays with hysteretic damping", Eur. Phys. J. Spec. Top. 231: 225-236 (2022). (2021).


Bountis, T., Skokos H. (2012)
"Complex Hamiltonian Dynamics", Springer Series in Complexity.

Thank you!